Proceedings of ASME Turbo Expo 2011
GT2011
June 6-10, 2011, Vancouver, British Columbia, Canada

GT2011-46315

APPLICATION OF A MULTISTAGE CASING TREATMENT IN A HIGH SPEED AXIAL COMPRESSOR TEST RIG

T. Kroeckel
Institute of Jet Propulsion and Turbomachinery
RWTH Aachen University
D-52062 Aachen, Germany
Email: kroeckel@ist.rwth-aachen.de

S.J. Hiller
MTU Aero Engines GmbH
D-80995 Munich, Germany
Email: sven-juergen.hiller@mtu.de

P. Jeschke
Institute of Jet Propulsion and Turbomachinery
RWTH Aachen University
D-52062 Aachen, Germany
Email: jeschke@ist.rwth-aachen.de

ABSTRACT

The subject of this paper is the experimental investigation of the overall performance and local aerodynamics of a 2.5 stage axial compressor test rig with a two stage casing treatment. Casing treatments are a well known method to aerodynamically stabilize the near stall compressor aerodynamics. However, in the past, casing treatments have only been applied to high aspect ratio front stages. This investigation puts the focus on the impact of advanced casing treatments applied to both rotors of a high speed compressor test rig. The rotors' geometric and aerodynamic features are identical to those seen in the rear stages of aircraft engine high pressure compressors. Based on experimental results, we explain the casing treatment's effect on the local flow phenomena as well as its influence on the compressor operability and performance. In order to clearly quantify the casing treatment's influence, all measurements are conducted twice: for the rig without casing treatments and for an identical rig with casing treatments.

The analysis of experimental data confirms that multistage casing treatments are able to significantly push the surge line towards higher pressure ratios and lower mass flow rates without any significant degradation of the peak efficiency. However, detailed flow analysis and the comparison of the configurations with and without casing treatments reveal that the flow is significantly redistributed by the effect of the casing.

The present effort was conducted as part of the EU integrated program for New Aero Engine Core Concepts (NEWAC).

INTRODUCTION

Design attributes for aircraft jet engines, such as low weight, high efficiency and safe operation, have always been the focus of engine manufactures, and have become even more important with increasing competition and rising fuel costs. Casing treatments are developed to address the demand for safe and stable compressor operation, but have an impact on other attributes as well. Over the last decades, various casing treatment designs have been developed to extend the operating range by pushing the surge line towards higher pressure ratios and lower mass flow rates [5]. Simple geometries such as single or multiple circumferential grooves [2][3] and axial or skewed slots [2][4], which are easy to manufacture, are most frequently studied but have a common drawback: the tendency to reduce the compressor efficiency. In contrast, more complex designs like recirculating casing treatments [5][6] have shown the potential for minimizing performance losses. It is well known that casing treatments have the potential to influence the compressor flow in the tip region, and are able to delay the breakdown of the tip leakage vortex which can lead to compressor stall. The beneficial impact of the casing treatments described above is limited to compressors with tip critical rotor blading [7].

In most cases, casing treatments were applied to single stage compressors or only to the front stage of multistage compressors. Some attempts to investigate multistage behavior were made by applying multiple stage recirculations [9].

For the present study, a self-recirculating casing treatment [10] (see Figure 1) was applied to both stages of a 2.5 stage compressor test rig (see Figure 2). The casing treatment used is an adaptation of a casing treatment applied to the TP400 aero engine as described in [6]. Pretest CFD studies were able to confirm the performance of the casing treatment.

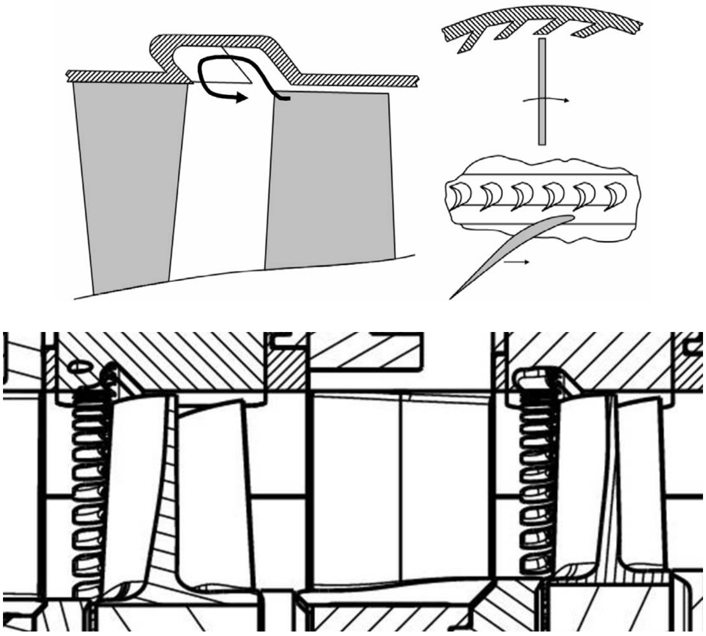

Figure 1. Conceptual drawing of the casing treatment [6][10] and the casing treatment installed at the test rig [11]

NOMENCLATURE

I,0	Measurement plane upstream of IGV	[-]
I,1	Measurement plane upstream of rotor 1	[-]
I,2	Measurement plane downstream of rotor 1	[-]
II,1	Measurement plane upstream of rotor 2	[-]
II,2	Measurement plane downstream of rotor 2	[-]
II,3	Measurement plane downstream of stator 2	[-]
SW	Smooth wall	[-]
CT	Casing treatment	[-]
A/D	Analog/Digital	[-]
IGV	Inlet Guide Vane	[-]
Ma	Mach number	[Ma]
P	Power input	[kW]
$\dot{Q}_V$	Heatflow	[kW]
PS, SS	Pressure side, suction side	[-]
R1, 2	Rotor 1, 2	[-]
RMS	Root mean square	[-]
S1, 2	Stator 1, 2	[-]
OP1, 2	Operating point 1, 2	[-]
T	Temperature	[K]
d	Diameter	[mm]
f	Frequency	[Hz]
h	Blade height	[mm]
ṁ	Absolute mass flow rate	[kg/s]
n	Nominal rotational speed	[rpm]
p	Static pressure	[Pa]
u	Circumferential velocity	[m/s]
w	Relative velocity	[m/s]
c	Absolute velocity	[m/s]

Greek symbols

Π	Pressure ratio	[-]
Δ	Delta	[-]
δ	Tip clearance	[mm]
η	Efficiency	[-]
ρ	Stage reaction	[-]
α	Absolute outflow angle	[°]
β	Relative outflow angle	[°]
κ	Ratio of specific heat	[-]

Subscripts

h	Hub
is	Isentropic
abs	Absolute
ax	Axial
ref	Reference
rel	Relative
t	Total, dimensionless time, tip
TM	Torque meter
bear	Bearing
I	Inlet
E	Exit
RMS	Root mean square

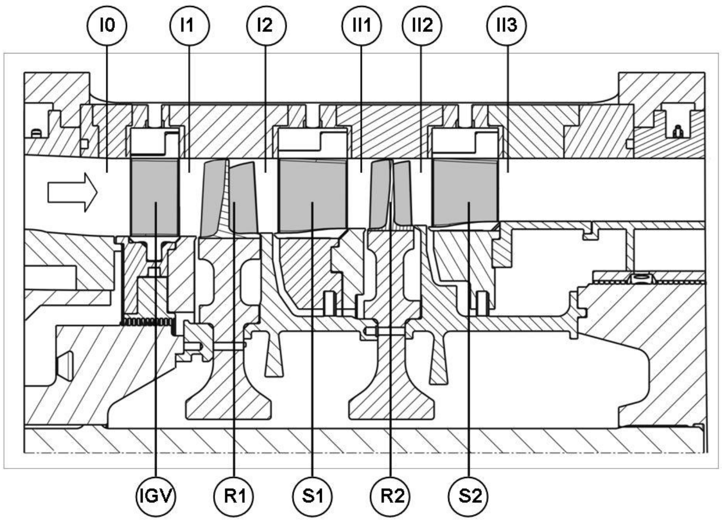

Figure 2. 2.5 stage compressor test rig

EXPERIMENTAL SETUP

The Institute of Jet Propulsion of the University of Aachen operates a 2.5 stage axial compressor test rig which is designed to represent the last stages of a modern jet engine high pressure compressor [8]. Figure 2 provides an overview of the actual rig setup including the indication of the measurement planes. Both rotors are integrally bladed. All stators have the same number of vanes and are equipped with tip and hub shrouds. In order to vary the relative circumferential position of an otherwise circumferentially fixed probe, all three stators can be rotated within the casing by a vane clocking system. However, the stagger angles remain fixed. In order to provide adequate inlet conditions a pressure controller is used to keep the total pressure at the compressor inlet constant for different mass flow rates. The total pressure distribution just upstream of the IGV is shown in Figure 3.

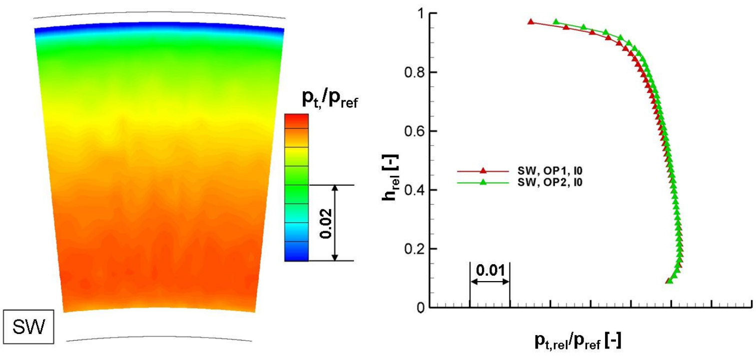

Figure 3. Total pressure distribution at compressor inlet OP1 (left), OP1 & OP2 (right)

In order to evaluate the influence of the casing treatment on the performance of the compressor, multiple measurement techniques were applied. Total pressure and total temperature rakes were placed both at the compressor inlet and outlet. A calibrated Venturi nozzle was used to determine the mass flow rate. The efficiency was evaluated by considering the torque of the rotor and the losses in the journal bearings.

$$\eta_{t,is,mech} = \frac{\kappa}{\kappa-1}\dot{m}RT_{t,I}\left[\Pi^{\left(\frac{\kappa-1}{\kappa}\right)}-1\right]/\left(P_{TM}-\dot{Q}_{V,bear}\right)$$

The efficiency at OP1 was determined with a relative uncertainty of 0.35%. This is confirmed by a formal error propagation assessment.

Nominal rotational speed	n	14,958	Rpm
Total pressure ratio	Π_t	1.67	-
Absolute mass flow	$\dot{m}$	7.70	kg/s
Isentropic efficiency	$\eta_{t,is}$	89.50	%
Power input	P	422	kW
Total temperature rise	ΔT_t	52.7	K
Inner casing diameter	d	385.43	mm
Rotor tip speed	u	302.40	m/s
Tip clearance R1	δ_{R1}	0.70	mm
Tip clearance R2	δ_{R2}	0.75	mm
Average stage reaction	ρ_h	0.69	-
Average aspect ratio (w/o IGV)	AS	0.95	-
Average hub/tip ratio	d_h/d_t	0.75	-
Reynolds number R1	Re_{R1}	9.0 E5	-
Average rel. rotor inlet Mach number (tip)	Ma_w	0.86	-
Average abs. stator inlet Mach number (hub)		0.56	-
Tip clearance relative to blade height rotor 1	δ/h	1.4	%
Tip clearance relative to blade height rotor 2	δ/h	1.6	%
Number of blades R1		24	-
Number of blades R2		32	-
Number of blades IGV, S1, S2		40	-
5-Hole Probe diameter	d_{5hp}	2.5	mm
Total pressure probe diameter	d_{tds}	2	mm

Table 1: Compressor specifications

All measurements were carried out on two rig configurations: a configuration with smooth walls, which represents the baseline, and the casing treatment configuration itself. Due to the fact that the rear stages of a high pressure compressor typically become critical at high rotor speeds, the majority of the measurements were carried out at an aerodynamic speed of 97% of the design speed. Excitations of the IGV ruled out the 100% speed. Therefore, measurements were taken at every measurement plane at two distinct operating points at the 97% speed line. The first operating point (OP1) was chosen to be at the point of maximum efficiency. Operating point 2 (OP2) was set to be as close as possible to the surge line of the smooth wall configuration provided that the rig was still running under stable conditions (see Figure 5). However, due to the casing treatments' effects the speed lines of both rig configurations are different. In order to get comparable results, the mass flow rate was kept constant for every operating point.

In addition to the standard compressor performance measurements radial and circumferential flow traverses were performed at each measurement plane. Five-hole probes with an integrated temperature sensor were traversed using automated traversing units. A high resolution grid of about 700 points with a circumferential extent ranging from 12 to 15 degrees was set up at each measurement plane. The densities of these grids were increased at the tip and hub region, and at regions of the stator wake. Measurements started as close as 1.5mm to the casing and ended with a 4.5mm stand off from the hub. High gradients which particularly appear in the stator wake have distorting effects on the measurement results of the five-hole probes. A method to compensate for this effect, as described by Vinnemeier [12], was applied during the processing of the pressure data.

An unsteady total pressure probe equipped with a high frequency pressure transducer (Kulite XCQ-62-25D) was used to unveil unsteady flow effects downstream of each rotor. Similar to the five-hole probe measurements, a grid of measurement points was implemented in an automated traversing routine. To reduce measurement time and since the influence of the casing treatment was only expected in regions close to the compressor wall, the measurement area was reduced to about 50% of blade height, starting with a 1mm offset at the compressor wall (see Figure 4). The compressor casing and hub are indicated by a solid line at every contour plot.

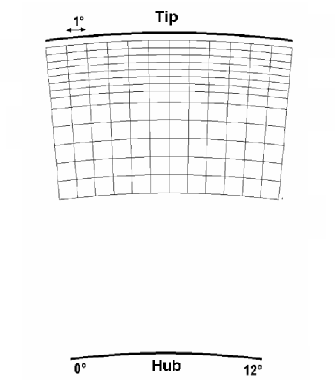

Figure 4. Measurement grid (unsteady total pressure probe)

The sample rate of the Kulite signal (359.424 kHz) was matched to the rotational speed of the rotor (14,958 min^{-1}) allowing the rotor to turn 0.25° between two samples. A single trigger at the rotor shaft started the recording of a block of 180 samples allowing three (R1) to four (R2) blade passes. At each full rotor revolution a new recording was started until 256 blocks were recorded. After this, the probe was traversed to the next measurement point. A multiplexer with a cut-off frequency of 109,650 Hz was used to amplify the Kulite signal. The recording of the amplified signal was realized by a PC with a built-in A/D converter card. Translating the sampled voltage values of the Kulite signal into pressure values, a method (Mass [13]) applying a temperature dependent pressure calibration of the sensor was used. In order to obtain an unsteady pressure distribution for the measurement grid, all 256 blocks of pressure values were ensemble averaged. The random part of the pressure signal (RMS), however, provides the best insights into the relevant flow phenomena and is therefore discussed in this paper.

COMPRESSOR MAP

In order to assess the influence of the casing treatments on the performance of the compressor, several measurements were carried out. The focus was on the four highest speed lines: 83%, 90%, 95% and 97%. A significantly extended surge margin could be achieved with the casing treatment configuration relative to the baseline with smooth casing walls (see Figure 5). The CT speed lines show a minor offset at de-throttled operating ranges. However, when the compressor is throttled, the configuration with the casing treatments tends to deliver a significantly higher pressure ratio at the same mass flow rate. This clearly proves the favorable influence of the casing treatments as they significantly increase the blade loading accompanied with a drastically enlarged stability but with only an insignificant loss in efficiency.

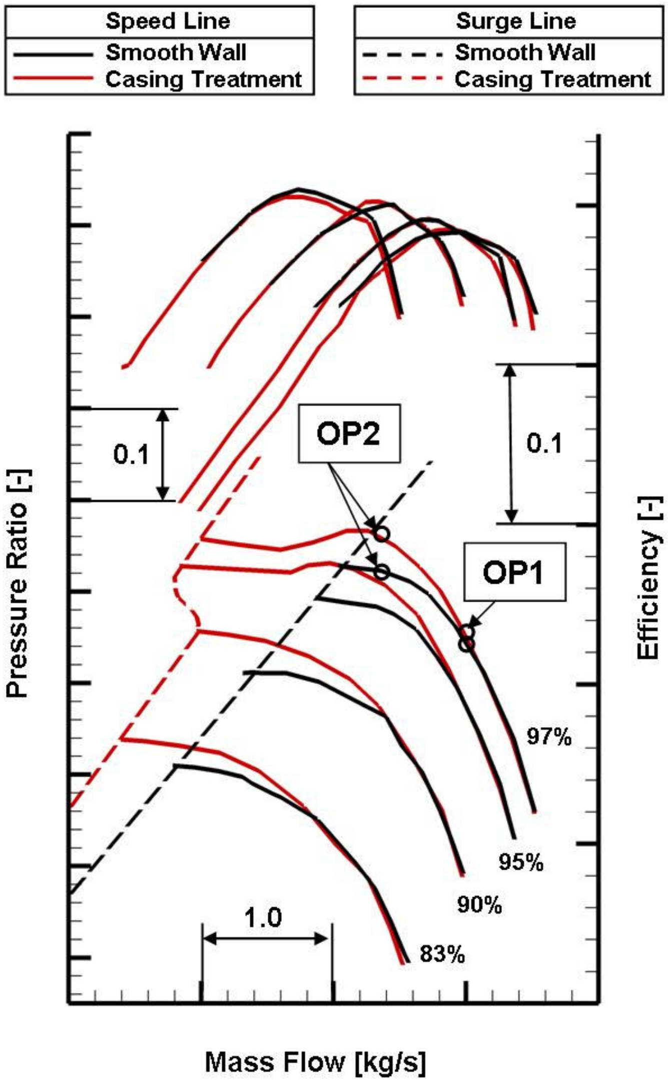

Figure 5. Compressor map

All speed lines measured at the baseline configuration indicate compressor stall each at the highest pressure ratio. A similar behavior, although at a higher pressure level, can be seen at the 83% and 90% speed lines for the compressor equipped with casing treatments. At 95% and 97% speed the compressor behaves differently. Instead, the compressor runs at secondary and tertiary characteristics as described by [14]. Once the speed line reached the peak with a horizontal pressure gradient, the compressor generated multiple stall cells. Further throttling led to a lower total pressure ratio - the compressor operated on secondary characteristics. Once the pressure began to rise again a full ring stall was established and the compressor operated on the tertiary characteristics until full surge occurred. This behavior could be traced by the installed unsteady pressure sensors, but it is not the subject of the current paper.

STEADY FLOW FIELDS

In order to understand the effects which led to the significant change of the compressor map, flow fields of the stages involved needed to be analyzed. Although the mass flow rate for each operating point was kept constant at both configurations, the compressor with casing treatments operated at higher pressure ratios. While the difference is relatively small at OP1, it rises with further throttling and reaches a maximum close to OP2. In order to explain the effects of the casing treatments, both the absolute and the axial velocity at the rotor outlet and the total pressure distribution at the stator outlet will be analyzed. This analysis is later complemented with circumferential averaged data.

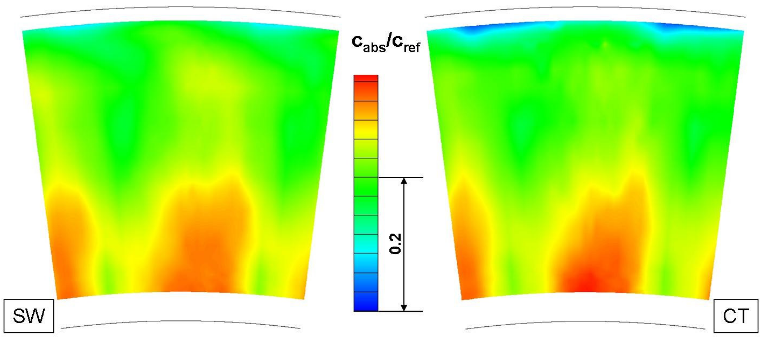

Figure 6. Absolute velocity at OP1 at plane I2 (rotor 1 exit)

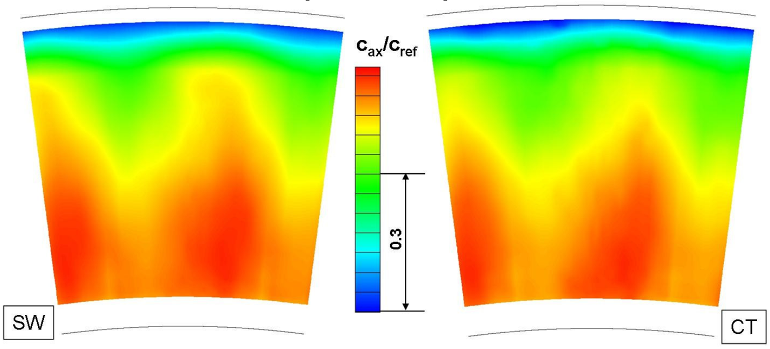

Figure 7. Axial velocity at OP1 at plane I2 (rotor 1 exit)

PLANE DOWNSTREAM ROTOR 1 AT OP1

The first effect of the casing treatment is observable downstream of rotor 1. Looking at the absolute velocity distribution (Figure 6) at the exit of the first rotor at OP1 gives a good impression regarding the emerging influence of the casing treatment. The circumferential expansion of this measurement plane is 12°. Two wakes of the IGV are clearly observable. The shape and extent of these wakes are about the same for both rig configurations. However, the first rotor's casing treatment causes a slight reduction of the absolute velocity at the region close to the rotor tip. On the other hand, regions of slightly increased absolute velocity are visible in the lower part of the measurement plane.

Although a direct influence of the casing treatment is not observable at the axial velocity distribution in Figure 7, an indirect indication is given at about 70% blade height where the axial velocity values drop slightly. This observation allows the conclusion that, for reasons of mass flow continuity, the axial velocity is slightly increased close to the casing (outside the measurement plane).

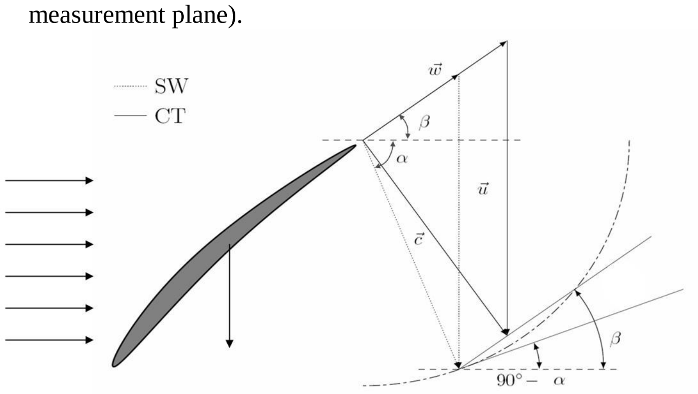

Figure 8. Velocity triangles at the rotor tip

Since the phenomenon of a lowered absolute velocity and a simultaneously raised axial velocity at the region of direct influence of the casing treatment is not very intuitive, the sketch in Figure 8 is used for explanation. Assuming the relative outflow angle β is fairly constant and the blockage effect of the tip leakage vortex is reduced by a casing treatment, both the axial velocity and the relative velocity rise according to Figure 7. While the circumferential velocity *u* of the rotor blade is constant, the absolute velocity drops as long as the relative velocity does not reach a certain level (indicated by the dashed circle). Although this may only be valid for specific blade geometries or staggering angles, the following section shows that it always remains true for the compressor studied in this work. In order to interpret the displayed velocities correctly it is important to consider the different scaling of the absolute velocity and axial velocity plots. Compared to the axial velocity the changes in absolute velocity are rather minor.

PLANE DOWNSTREAM STATOR 1 AT OP1

The total pressure distribution downstream of stator one (Figure 9) helps complete the picture of the changed flow pattern. The wake of stator one produces a distinct region of low total pressure. For the smooth wall configuration, the extent of the wake is reasonably constant with a small expansion close to the casing in the region of a corner vortex.

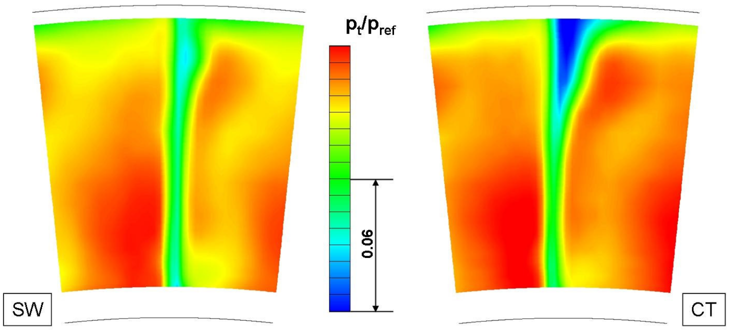

Figure 9. Total pressure at OP1 at plane II1 (stator 1 exit)

The wake at the casing treatment configuration has an increased extent at the tip region indicating a raised stator 1 loading. An additional difference (Figure 9) is the raised total pressure in the upper region of the main passage of the casing treatment configuration as a result of a changed inflow profile of the stator and a reduced intensity of the rotor 1 tip leakage vortex and therefore less total pressure loss at the stator passage.

PLANE DOWNSTREAM ROTOR 2 AT OP1

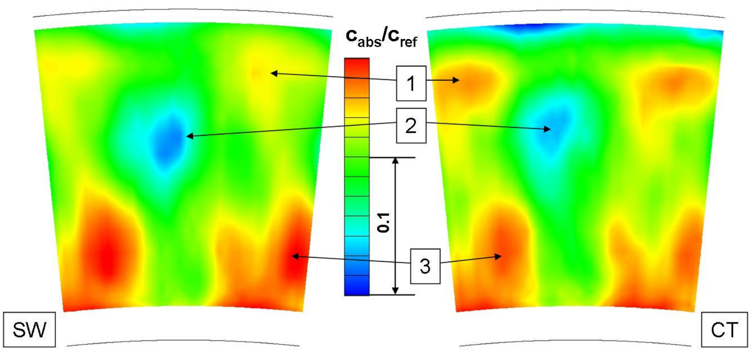

Figure 10. Absolute velocity at OP1 at plane II2 (rotor 2 exit)

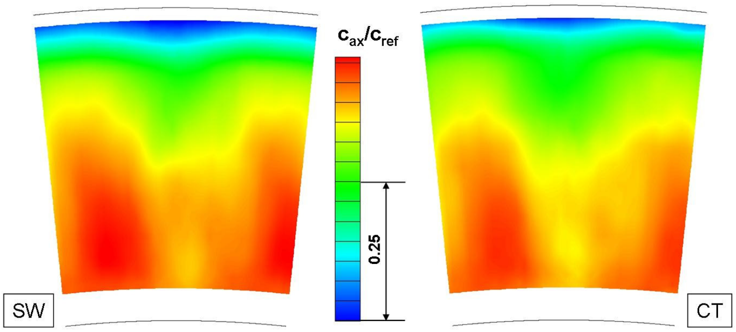

Figure 11. Axial velocity at OP1 at plane II2 (rotor 2 exit)

While the flow field at the outlet of the second rotor has similarities to the flow field of the first rotor, the effects of the casing treatment at rotor 1 are transported downstream and overlap with the effects of the casing treatment at rotor 2. Looking at the absolute velocity of the smooth wall configuration (see Figure 10), a wake of stator one produces a local minimum (2) at about 60% blade height while the main passage flow of stator 1 creates a local maximum (3) at 30% and another smaller maximum (1) at 90% blade height. The local effect of the casing treatment above rotor 2 resulted in a reduction of the absolute velocity at the tip region.

Although slightly changed due to the alternated inflow at rotor 2, these maxima and minima were still visible in the casing treatment configuration. The minimum (2) caused by the stator wake is shifted towards the blade tip. While the upper local maximum (1) is more pronounced and moved away from the tip, the lower one (3) maintains its position but with a reduced magnitude. In Figure 11, the axial velocity distribution shows a stronger influence of the casing treatment at rotor 2. Close to the tip, the velocity is increased while it is reduced at the lower end of the measurement plane.

PLANE DOWNSTREAM ROTOR 1 AT OP2

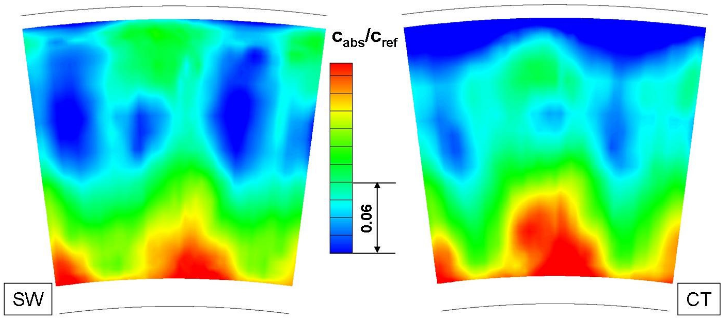

Figure 12. Absolute velocity at OP2 at plane I2 (rotor 1 exit)

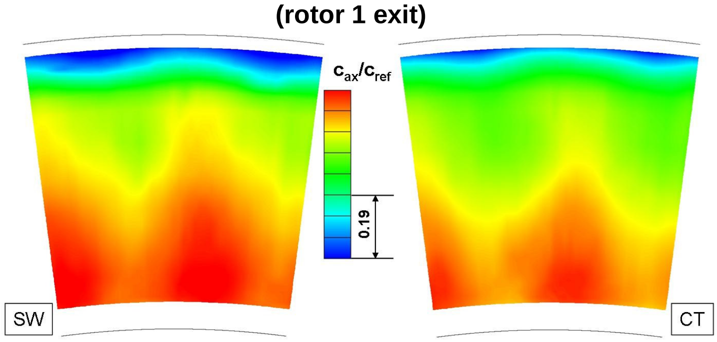

Figure 13. Axial velocity at OP2 at plane I2 (rotor 1 exit)

The second operating point was chosen close to the surge line of the smooth wall configuration. As seen in the compressor map, keeping the same mass flow rate, the configuration with casing treatments operated at a much higher pressure ratio. The flow pattern downstream of rotor 1 is illustrated by the absolute and axial velocity distribution in Figure 12 and Figure 13. Similarly to OP1, two wakes caused by IGV are observable. But unlike the first operating point, here the influence of the casing treatment was much stronger and the axial velocity close to the compressor wall was significantly increased by the casing treatment. At the region outside of the direct influence of the casing treatment, a uniform reduction of the axial velocity is observable.

PLANE DOWNSTREAM STATOR 1 AT OP2

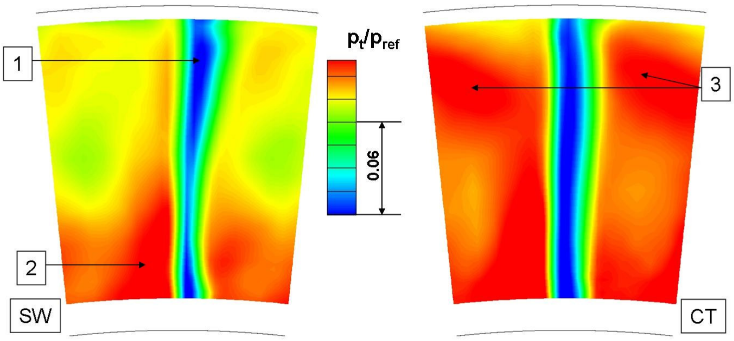

Figure 14. Total pressure at OP2 at plane II1 (stator 1 exit)

Compared to OP1, the total pressure downstream of stator 1 (see Figure 14) of the smooth wall configuration showed a less even distribution. The high absolute velocity at the exit of rotor 1 causes an enlarged wake (1) at the tip region (Figure 14 left) - a sign of increased losses at the stator passage. A region of relatively high pressure (2) was situated close to the hub while lower pressures can be seen at the middle and tip. Applying a casing treatment to the compressor changed the inflow profile in front of the stator and reduced the intensity of the tip leakage vortex, which caused a total pressure rise (3) at the upper part of the measurement plane at the stator exit.

PLANE DOWNSTREAM ROTOR 2 AT OP2

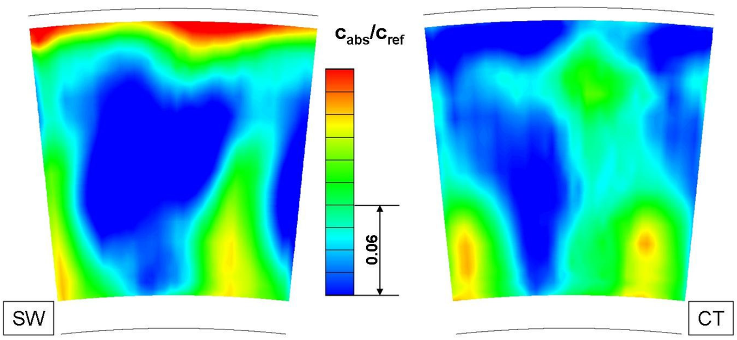

Figure 15. Absolute velocity at OP2 at plane II2 (rotor 2 exit)

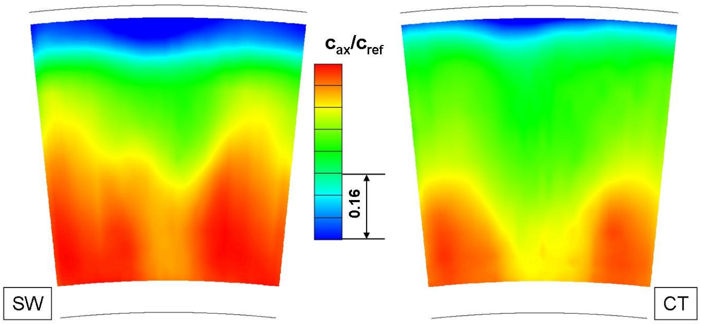

Figure 16. Axial velocity at OP2 at plane II2 (rotor 2 exit)

The blocking effect of the tip leakage vortex led to a further reduction of the axial velocity close to the casing (Figure 16 left) and became most apparent at the exit flow of rotor 2. With an axial velocity at a very low level, the circumferential part of the velocity gets more dominant resulting in relatively high absolute velocity values at the tip (see Figure 15). Compared to rotor 1, the redirection of the flow at the tip is stronger at the second rotor - an indication of higher loading at rotor 2. By applying the casing treatment to the compressor, the blocking effect of the tip leakage vortex was massively reduced and the flow field changed dramatically: with a reduced absolute velocity and increased axial velocity at the rotor tip. While the effects of the local CTs were limited to the upper 80% of the blade height, any significant changes below 80% can be linked to the downstream effect of the CT at rotor 1. Therefore, a second effect, a clear sign of the downstream influence of the casing treatment at rotor 1 can be seen in Figure 15: the absolute velocity was notably higher at about 70% blade height.

CIRCUMFERENTIAL AVERAGED DATA

Although most of the effects caused by the casing treatment were described in the previous section, an even deeper understanding can be reached by comparing both compressor configurations at both operating points. To achieve this, the relevant values were circumferentially averaged and displayed in several plots.

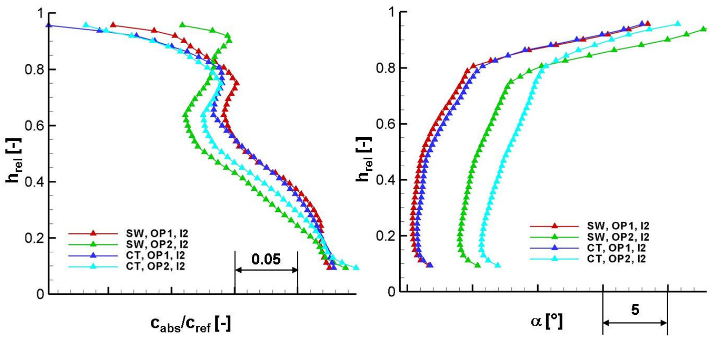

Figure 17. Absolute velocity (left), absolute outflow angle (right) at plane I2 (rotor 1 exit)

The absolute velocity at both operating points of the smooth wall and casing treatment configuration is displayed in Figure 17. The redistribution effect described in the above section becomes visible again. An increased influence of the casing treatment with reduced blade loading can be observed at the tip region. Looking at the absolute outflow angle in Figure 17, a different behavior can be seen due to the direct influence of the casing treatment close to the tip (reduced angle) compared to the region without this influence (increased angle).

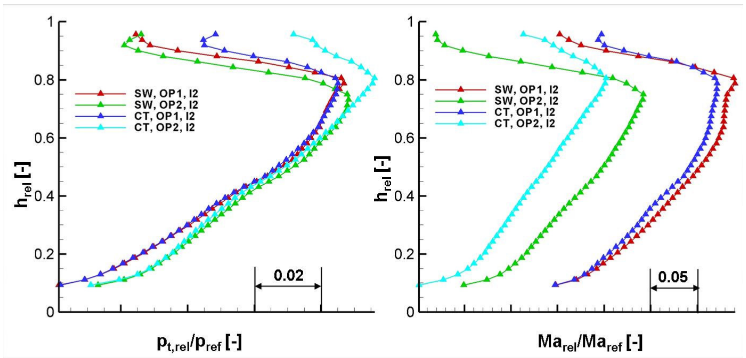

Figure 18. Relative total pressure and relative Mach number at plane I2 (rotor 1 exit)

Further differences become apparent when considering the measured data relative to the rotor rotation. The relative total pressure and the relative Mach number at the exit of rotor 1 (Figure 18) underlines the phenomena described earlier. Due to the influence of the casing treatment the energy conversion at the rotor is higher. The relative total pressure, as well as the relative Mach number, was raised accordingly at the tip of the blade. It becomes very obvious that about 20% of the outer blade section is under the direct influence of the casing treatment flow.

While throttling the smooth wall compressor, the outermost section of the blade generated increased pressure losses. The stage at which a casing treatment was installed behaved differently. Total pressure was increased at the tip section. At the same time the shape of the pressure and Mach number curves at OP1 (Figure 18) also indicates that the casing treatment had no effect on the main flow of the compressor. At the tip region, both curves showed characteristic radial gradients as a result of the tip leakage flow. Throttling the casing treatment configuration (OP2) this characteristic disappeared almost completely but remained at the smooth wall compressor. This confirms the significant effect of the casing treatment on the tip leakage flow. The shape of the total pressure at OP1 also explains why the selected casing treatment configuration is nearly efficiency neutral.

Any additional loss mechanism linked to the influence of the casing treatment is not visible. In contrast, the circumferential slot affects the tip clearance flow in a way that the blade tip generated less losses.

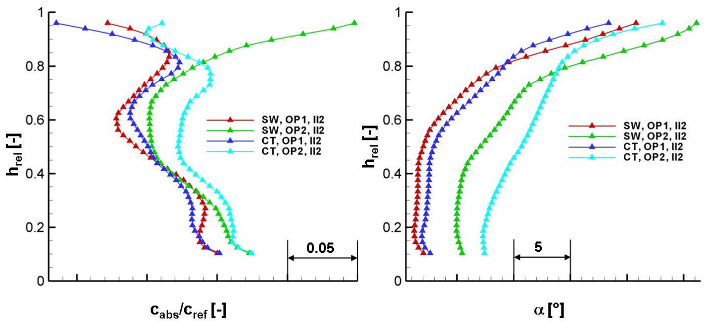

Figure 19. Absolute velocity (left), absolute outflow angle (right) at plane II2 (rotor 2 exit)

Figure 19 is similar to Figure 17 but includes the additional effect of the downstream influence of the casing treatment at rotor 1. The absolute velocity outside of the direct influence of the casing treatment was changed due to the raised total pressure at the exit of stator 1. Furthermore, comparing the relatively large difference in outflow angles close to the tip of rotor 2 (OP2) to the smaller difference at rotor 1 (Figure 17), it can be concluded that rotor 2 is loaded slightly higher. Therefore, the casing treatment has an even larger effect on rotor 2.

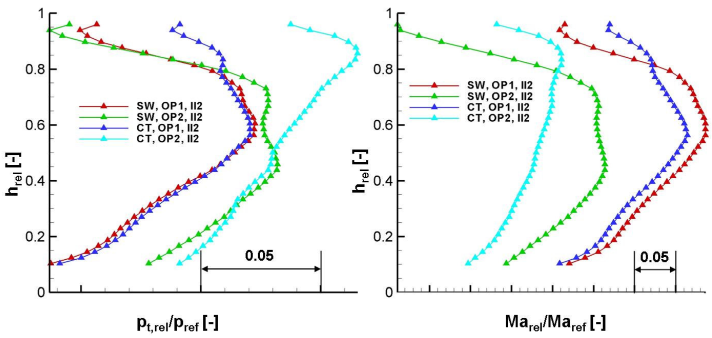

Figure 20. Relative total pressure and relative Mach number at plane II2 (rotor 2 exit)

The relative data recorded downstream of rotor 2 emphasizes the effect of the first casing treatment on the flow of the second rotor. The total pressure at OP2 changed above 50% blade height, which is far beyond the influence of the local casing treatment. While relative Mach number of the smooth wall configuration shows a curved distribution at 80% blade height, it straightens out for the casing treatment configuration. Again, this can be explained by the downstream influence of casing treatment at rotor 1.

In summary, a significantly improved energy transfer process at the rotor blades was established by both casing treatments resulting in significantly increased relative total pressure and relative Mach number. This effect can also be seen on the compressor map (Figure 5) by means of the higher pressure ratio of the casing treatment configuration. It can be concluded that casing treatments in a multistage configuration harmonizes the blade loading along the span at the cost of slightly higher blade loading level in general. The same operating point (mass flow and pressure ratio) can only be reached by lowering the aerodynamic speed.

UNSTEADY FLOW FIELD

In order to determine the influence of the casing treatment on the rotor flow field, traverses with high response total pressure probes were used in measurement planes I,2 and II,2, just downstream of each rotor. The RMS values of the time resolved total pressure are considered to be a good indicator of the size and strength of the rotor tip vortex. Again, data were recorded with and without a casing treatment at the two operating points OP1 and OP2 on the 97% speed line. The recorded data are displayed as time-averaged RMS-values of unsteady total pressure distribution. Processing the recorded data lead to the following figures where the viewpoint is fixed relative to the moving rotor blade and all fluctuations are averaged over time. The rotor flow field can be seen as the averaged fluctuation level, where due to the averaging process no influence of the stator becomes visible.

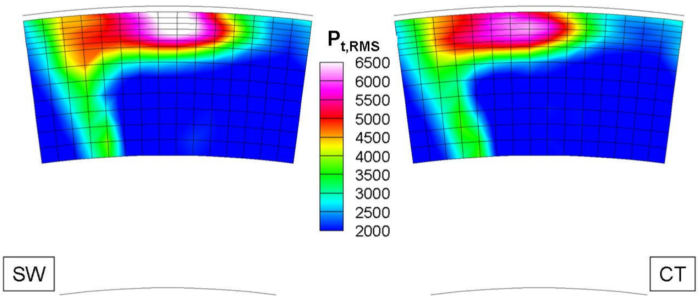

Figure 21. RMS of the total pressure at OP1 at plane I2 (rotor 1 exit)

Looking at the data shown in Figure 21, the tip leakage vortex can be clearly seen at the region close to the compressor wall. The vortex was generated at a blade outside of the measurement plane and was partially merging with the wake of the next blade. The steady results described in the previous section predicted a very small influence of the casing treatment on the blockage effect of the tip vortex at rotor 1. Figure 21 completes this picture and shows a slight reduction of the vortex strength for the casing treatment configuration.

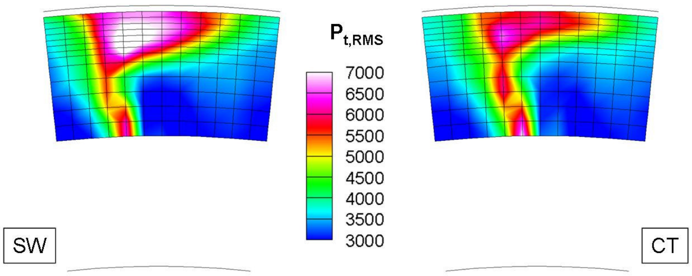

Figure 22. RMS of the total pressure at OP1 at plane II2 (rotor 2 exit)

From the section above, rotor 2 is known to be more highly loaded than rotor 1. The conclusion that the influence of the casing treatment is driven by the blade load is emphasized by Figure 22. The size of the leakage vortex of rotor 2 at OP1 was already significantly reduced through the casing treatment.

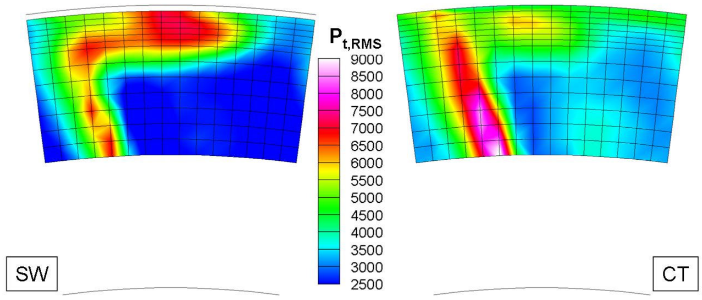

Figure 23. RMS of the total pressure at OP2 at plane I2 (rotor 1 exit)

At OP2, the compressor was more highly loaded and the overall fluctuation level (RMS-value) was higher. Therefore, the scaling of the RMS-values had to be adjusted accordingly. Fluctuations at the rotor wake were increased as well as those at the vortex. This was a sign of higher blade loading for the smooth wall configuration. On the right side of Figure 23, the rotor wake of the casing treatment configuration becomes dominant and, as expected, the vortex is further reduced.

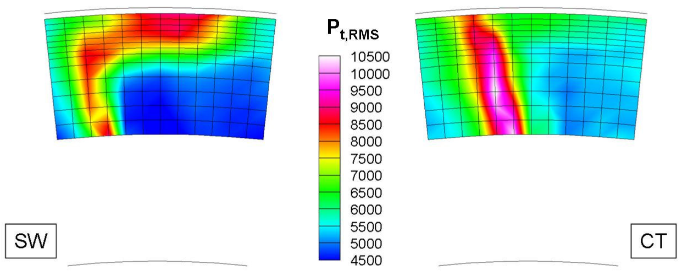

Figure 24. RMS of the total pressure at OP2 at plane II2 (rotor 2 exit)

The flow field at the exit of rotor 2 shows the most definite evidence of an interaction between the casing treatment and the tip leakage vortex (Figure 24): the vortex was reduced to a level where its fluctuations are no higher than the average fluctuations of the main flow. The rotor wake becomes the dominant flow pattern at OP2.

CONCLUSIONS

1. The surge margin of a high tip loading multistage compressor can be effectively increased by the use of casing treatments applied to the casing of each rotor.
2. The casing treatment causes a radial redistribution of the compressor flow. The mass flow at the tip, the region of direct influence of the casing treatment, is raised while the mass flow below that region is reduced.
3. A well designed recirculating casing treatment does not have degrading effects on compressor efficiency at the aerodynamic design point.
4. The casing treatment has an influence on stages further downstream.
5. The casing treatment, also in a multistage configuration, harmonizes the blade loading along the span at the cost of slightly higher blade loading level in general.
6. The casing treatment changes the outflow angle at the rotor tip by reducing the absolute velocity and, at the same time, increasing the axial velocity.
7. Clearly, with higher loading the casing treatment has a bigger impact on the main flow.
8. The casing treatment has a direct influence on the tip leakage vortex: at operating points close to the surge point (of the SW configuration), the vortex is significantly reduced.

ACKNOWLEDGEMENTS

The authors would like to thank MTU Aero Engines GmbH and the other NEWAC partners for permission to publish this paper. The authors also wish to thank the E.U. for supporting this project - the work was founded under the E.U. contract number FP6-030876.

REFERENCES

[1] Hathaway, M.D., 2007, “Passive endwall treatments for enhancing stability”, NASA Report TM-2007-214409

[2] Osborn, W.M, Lewis, G.W., Heidelberg, L.J., 1971, “Effect of several porous casing treatments on stall limit and overall performance of an axial compressor rotor”, NASA Report TN 6537

[3] Houghton, T., Day, I., 2009, “Enhancing the stability of subsonic compressors using casing grooves”, ASME paper GT2009-59210

[4] Wilke, I., Kau H-P., 2004, “A numerical investigation of the flow mechanisms in a high-pressure compressor front stage with axial slots”, ASME J. Turbomachinery

[5] Zscherp, C., 2008, “Aerodynamische Verdichterauslegung unter Berücksichtigung stabilitätsverbessernder Maßnahmen”, Sierke Verlag, Goettingen, ISBN 978-3-86844-095-9

[6] Engel, K., Zscherp, C., Wolfrum, N., Nürnberger, D., Kügeler, E., 2009, “CFD Simulations of the TP400 IPC With Enhanced Casing Treatment in Off-Design Operating Conditions”, ASME paper GT2009-60324

[7] Van de Wyer, N., Farkas, B., Desset, J., Brouckaert, J.F., Thomas, J.-F., Hiernaux, S., 2010, “Experimental Investigation of the Steady and Unsteady Flow Field in a Single Stage Low Pressure Axial Compressor with a Circumferential Groove Casing Treatment”, ASME paper, GT2010-23474

[8] Ernst, M., Michel, A., Jeschke, P., 2009, “Analysis of Rotor-Stator-Interaction and Blade-to-Blade Measurements in a Two Stage Axial Flow Compressor”, ASME paper GT2009-59371

[9] Strazisar, A.J., Bright, M.M., Thorp, S., Culley, D.E., Suder, K.L., 2004, “Compressor stall control through endwall recirculation”, ASME paper, GT2004-54295

[10] Seitz, P., 2005, “Recirculation Structure for Turbo Chargers”, US Patent 6,935,833 B2, MTU Aero Engines GmbH, Munich, Germany

[11] Kroeckel, T., 2010, “Multistage Casing Treatment at High Pressure Compressor Rear Stages”, Workshop Presentation, European Workshop on New Aero Engine Concepts

[12] Vinnemeier, F., Simon, L., Koschel, W., 1990, “Korrektur des Kopfgeometrieeinflusses einer Fünfloch-Drucksonde auf die Messergebnisse”, TM 57 Oldenbourg Verlag

[13] Maas, M., 1995, “Kalibrierung von Halbleiter-Drucksonden”, DLR-Mitteilung 95-03

[14] Cumpsty, N. A., 2004, “Compressor Aerodynamics”, Krieger Publishing Company

